Biophysical Journal
Article

Biophysical Society

Circulating cell clusters aggravate the hemorheological abnormalities in COVID-19

Elahe Javadi,[1] He Li,[2,3,*] Ander Dorken Gallastegi,[4] Galit H. Frydman,[4,5] Safa Jamali,[1,*] and George Em Karniadakis[2,6,*]

[1]Department of Mechanical and Industrial Engineering, Northeastern University, Boston, Massachusetts; [2]School of Engineering, Brown University, Providence, Rhode Island; [3]School of Chemical, Materials and Biomedical Engineering, University of Georgia, Athens, Georgia; [4]Division of Trauma, Emergency Surgery and Surgical Critical Care at the Massachusetts General Hospital, Boston, Massachusetts; [5]Department of Biological Engineering at the Massachusetts Institute of Technology, Cambridge, Massachusetts; and [6]Division of Applied Mathematics and School of Engineering, Brown University, Providence, Rhode Island

ABSTRACT Microthrombi and circulating cell clusters are common microscopic findings in patients with coronavirus disease 2019 (COVID-19) at different stages in the disease course, implying that they may function as the primary drivers in disease progression. Inspired by a recent flow imaging cytometry study of the blood samples from patients with COVID-19, we perform computational simulations to investigate the dynamics of different types of circulating cell clusters, namely white blood cell (WBC) clusters, platelet clusters, and red blood cell clusters, over a range of shear flows and quantify their impact on the viscosity of the blood. Our simulation results indicate that the increased level of fibrinogen in patients with COVID-19 can promote the formation of red blood cell clusters at relatively low shear rates, thereby elevating the blood viscosity, a mechanism that also leads to an increase in viscosity in other blood diseases, such as sickle cell disease and type 2 diabetes mellitus. We further discover that the presence of WBC clusters could also aggravate the abnormalities of local blood rheology. In particular, the extent of elevation of the local blood viscosity is enlarged as the size of the WBC clusters grows. On the other hand, the impact of platelet clusters on the local rheology is found to be negligible, which is likely due to the smaller size of the platelets. The difference in the impact of WBC and platelet clusters on local hemorheology provides a compelling explanation for the clinical finding that the number of WBC clusters is significantly correlated with thrombotic events in COVID-19 whereas platelet clusters are not. Overall, our study demonstrates that our computational models based on dissipative particle dynamics can serve as a powerful tool to conduct quantitative investigation of the mechanism causing the pathological alterations of hemorheology and explore their connections to the clinical manifestations in COVID-19.

SIGNIFICANCE Inspired by a recent flow imaging cytometry study of the blood samples from patients with coronavirus disease 2019, we perform a computational investigation of the dynamics of different types of circulating cell clusters, namely white blood cell (WBC) clusters, platelet clusters, and red blood cell clusters over a range of shear flows and quantify their impact on the viscosity of the blood. Our simulation results suggest that formation of WBC and red blood cell clusters could cause a significant increase in the local viscosity of the blood, whereas the impact of platelet clusters on the rheology is negligible. This finding provides a possible explanation for the clinical finding that the number of WBC clusters is significantly correlated with thrombotic events.

INTRODUCTION

Coronavirus disease 2019 (COVID-19) caused by the severe acute respiratory syndrome coronavirus 2 (SARS-CoV-2) virus continues to be a major global health concern. In addition to affecting gastrointestinal and respiratory tracts, COVID-19 infections could increase the risk of intravascular clot formation and disseminated intravascular coagulation in patients with COVID-19 (1). For instance, Kelak et al. (2) reported a 31% rate of thrombotic complications among 184 patients with proven COVID-19 pneumonia. This finding was further confirmed by a number of subsequent studies showing the strong correlation between COVID-19 and thromboembolic events (3–6). It appears that thrombosis affects different parts of the human body,

Submitted April 7, 2022, and accepted for publication August 22, 2022.

*Correspondence: he_li@brown.edu or s.jamali@northeastern.edu or george_karniadakis@brown.edu

Editor: Padmini Rangamani.

https://doi.org/10.1016/j.bpj.2022.08.031

particularly the peripheral deep vein vessels, which is manifested by acute limb ischemia, a common incident occurring to patients with COVID-19 in northern Italy (7). Moreover, a notable association between COVID-19 and acute myocardial infarction induced by coronary artery obstruction or rupture of a preexisting atherosclerotic plaque was also reported in many clinical studies (8–12). All three components of the Virchow triad (13), namely endothelial injury, blood stasis, and hypercoagulability, are likely to contribute to COVID-induced thrombosis. Direct invasion of endothelial cells by SARS-CoV-2 causes endothelial injury that may initiate thrombosis at different vital organs (14). Blood stasis may result from the immobilization of hospitalized patients (15). An aggressive viral infection also causes coagulation abnormalities, which is manifested as elevated circulating prothrombotic factors such as von Willebrand factor, factor VIII, fibrinogen, neutrophil extracellular traps, prothrombotic microparticles, and anionic phospholipids (16). Accumulating evidence from autopsies (17–21) has shown that these prothrombotic factors not only can trigger thrombosis at macroscale but also contribute to the formation of microvascular thrombi within vital organs, such as the lungs, liver, kidney and heart, leading to microvascular dysfunction and multiorgan failure in patients with severe cases of COVID-19 (22). Emerging clinical studies have further shown that microthrombi are common microscopic findings in patients with COVID-19 at different stages of the disease course, implying that they may function as the primary drivers in disease progression (19,23).

In addition to the prothrombotic factors associated with Virchow triad, abnormal blood rheology has been connected with the increased risk of thrombotic events (24–26). A number of prior clinical studies have associated the altered hematocrit, the abnormal red blood cell (RBC) biomechanics, and enhanced RBC adhesion with both arterial thrombosis, which refers to blood clots formed in arteries, and venous thrombosis, a blood clot that develops in veins, in different RBC disorders, such as sickle cell disease (27), thalassemia (28), diabetes mellitus (29), and hemolytic anemias (30). However, there are few experimental investigations on the impact of COVID-19 infection on the blood rheology because fresh COVID-19 blood samples are limited to access due to the infectious nature of SARS-CoV-2. In a recent clinical study, Kubankova et al. (31) investigated the biomechanics of blood cells of patients with COVID-19 and reported that there is an increased heterogeneity of deformation and size in COVID-19 RBCs, although their mean values do not vary significantly from the RBCs of normal subjects. Subsequently, Nader et al. (32) discovered increased blood viscosity and RBC aggregation in patients with COVID-19, and their studies suggested that the increase in the viscosity is primarily driven by the RBC hyper-aggregation due to the increased level of fibrinogen. Recent clinical studies have discovered various types of circulating cell clusters (CCCs), like white blood cell (WBC) clusters, platelet-WBC clusters, and platelet-RBC aggregates, in the blood samples of patients with COVID-19 (33–36). These CCCs are thought to initiate the growth of thrombosis and may cause end-organ damage and thus have been associated with clinical outcomes of patients with COVID-19 (33). However, the underlying mechanism of how these CCCs alter the blood rheology and affect the microcirculation is still elusive.

Blood rheology is commonly assessed through rheometries that measure the rate of fluid flow by applying a force like in rotational rheometers or measure the force required to apply a specific flow rate, like in capillary viscometers (37). These viscosity measurement techniques usually face challenges of accurately measuring the blood viscosity at low shear rates due to the blood clotting and formation of a cell depletion layer next to wall leading to an exponentially decreasing apparent viscosity (38). In the last two decades, computational modeling of blood cells and blood flow has been widely employed to provide complementary information for experimental observations and offer insights for the biological processes that cannot be directly observed in clinical and experimental studies (see reviews (39–43)). Particularly, computational models have been used to predict of blood viscosity under a broad range of shear rates for normal and diseased blood (44–48). It is worth mentioning that Fedosov et al. (44) presented a multiscale modeling technique on blood rheology that could model the shear-thinning behavior of the normal blood. Lei and Karniakadis (48) predicted the increased blood viscosity of sickle blood where the stiffness and morphologies of RBCs are altered due to the polymerization of sickle hemoglobin inside RBCs (49–52). Subsequently, Chang et al. (53) and Liu et al. (47) performed computational investigations of the abnormal blood rheology in diabetic and heated blood, respectively. In recent studies, Javadi et al. (45,46,54) elaborated on the connection between the rheology of RBC suspension and its microscopic properties such as structure or arrangement, cell viscoelastic properties, local dynamics, and intrinsic cell interactions (e.g., RBC aggregation) in hyperviscosity syndrome.

Although extensive studies have been conducted to quantify how changes in major biophysical factors like cell counts, stiffness, aggregation, and elevated serum viscosity can affect blood viscosity, the impact of CCCs has not been investigated in detail. Inspired by observations made using flow imaging cytometry in (33), herein, we perform computational simulations to investigate the dynamics of different types of CCCs under various shear flows, aiming to quantify their impact on the hemorheology. In addition, we evaluate critical shear rates that can cause the breakup of these CCCs to provide insights on the correlation between the hemodynamics and the formation of these CCCs as well as their adverse impact on the blood perfusion in microcirculation.

MATERIALS AND METHODS

Images of CCCs

Under Institutional Review Board approval (protocol #2020P001364), discarded whole-blood samples collected in EDTA vacutainer tubes were collected from patients presenting to the Massachusetts General Hospital (Boston, MA, USA) between July and August 2020. COVID-19 positivity was defined as having a positive SARS-CoV-2 PCR result. Blood samples were fixated with 4% paraformaldehyde, washed for removal of plasma, and stored at 4°C in phosphate-buffered saline. All samples were processed within 12 h of blood draw. Flow cytometry data, as shown in Fig. 1, illustrated the presence of different types of CCCs in the blood samples, such as RBC clusters, platelet clusters, WBC clusters, etc.

Simulation model and method

Numerous multiscale computational models for describing RBC biomechanics have been developed to simulate the biological processes associated with RBC physiology and pathology. The protein-level RBC models, such as in (55–58), are capable of investigating the pathological alterations of the biomechanics of diseased RBCs resulting from either protein defects or virus invasion (59–64). However, these models cannot be employed to simulate blood cell suspensions or blood flow due to the high computational cost. On the other hand, highly efficient cellular-level RBC and platelet models developed based on (65) have been widely used to study multiscale biological phenomena from single RBC mechanics (47,61,66,67) to blood flow dynamics (68–71). Following our previous studies (45,46), we apply a cellular-level RBC model (72) developed based on dissipative particle dynamics (DPD) (73) to model blood suspension, including plasma, RBCs, platelets, and WBCs. In the DPD method, the equations of motion for each particle i with mass m_i is determined by the sum of pair interactions f_i with the surrounding particles j that composed of a conservative force (F_{ij}^C), a dissipative force (F_{ij}^D), and a random force (F_{ij}^R) given by

$$\mathrm{F}_{ij}^{C} = a_{ij}\left(1 - r_{ij}/r_c\right)\widehat{r}_{ij}\, for\ r_{ij} \le r_c\ 0\, for\ r_{ij} > r_c, \quad (1)$$

$$\mathrm{F}_{ij}^{D} = -\gamma\omega_d\left(r_{ij}\right)\left(\widehat{v}_{ij}.\widehat{r}_{ij}\right)\widehat{r}_{ij}, \quad (2)$$

$$\mathrm{F}_{ij}^{R} = \sigma\omega_r\left(r_{ij}\right)\frac{\xi_{ij}}{\sqrt{dt}}\widehat{r}_{ij}, \quad (3)$$

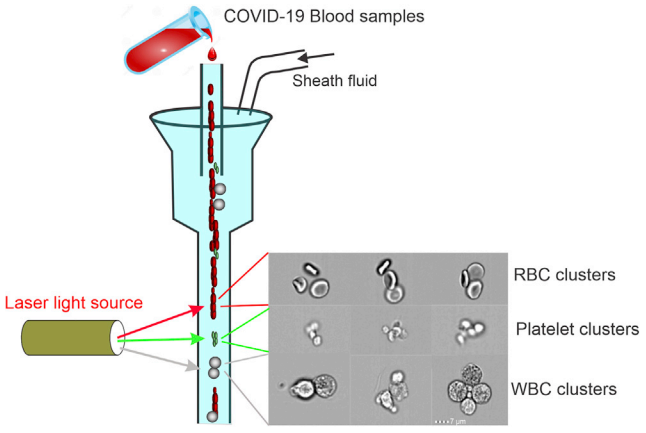

FIGURE 1 Various types of CCCs, such as RBC clusters, platelet clusters, and WBC clusters, were observed through imaging flow cytometry analysis of blood samples of COVID-19 patients. To see this figure in color, go online.

where $\widehat{r}_{ij} = \frac{r_{ij}}{r_{ij}}$, $\widehat{v}_{ij} = v_i - v_j$ and the parameters a_{ij}, γ, and σ are the conservative, dissipative, and random force coefficients where $\sigma^2 = 2\gamma k_b T$ (k_b is the Boltzmann constant and T is the temperature of the system). The weight function $\omega_r(r_{ij}) = (1 - r_{ij}/r_c)^k$, with $k = 1$ and $\omega_d = \omega_r^2$. The model parameters involved in Eqs. 1–3 are listed in Table S1.

Blood cell model

The membrane of the blood cells, including RBCs, platelets, and WBCs, are modeled as a set of N_v particles with the coordinates X_i, $i \in 1, \ldots, N_v$ in a two-dimensional triangulated network, as illustrated in Fig. 2. This elastic cell model was first proposed by Boey et al. (74) to study the deformation of RBCs under micropipette aspiration and then was integrated with different flow solvers, such as DPD (75), multiparticle collision dynamics (76,77), and lattice Boltzmann method (71,78) to simulate the dynamics of RBCs in microchannels. The free energy of each cell is defined as

$$V\{x_i\} = V_s + V_b + V_a + V_v, \quad (4)$$

where V_s is the elastic energy and is defined by

$$V_s = \sum_{j\epsilon 1\ldots N_s}\left[\frac{K_B T l_m\left(3x_j^2 - 2x_j^3\right)}{4p\left(1 - x_j\right)} + \frac{k_p}{(n-1)l_j^{n-1}}\right], \quad (5)$$

where K_BT is the energy unit, l_m is the maximum spring extension, $x_j = l_j/l_m \epsilon(o,1)$, p is the persistence length, l_j is the length of the spring j, k_p is the spring constant, and n is a specified exponent. N_s is the number of elastic bonds that connect the vertices. V_b is the bending energy of the cell membrane and is defined as

$$V_b = \sum_{j\epsilon 1\ldots N_s} K_b\left[1 - \cos\left(\theta_j - \theta_0\right)\right], \quad (6)$$

where K_b is the bending constant, θ_j is the instantaneous angle between two adjacent triangles having the common edge j, and θ_0 is the spontaneous angle. V_a and V_v define the area and volume conservation constraints, respectively, and they are given by

$$V_a = \sum_{j\epsilon 1\ldots N_t}\frac{K_d\left(A_j - A_0\right)^2}{2A_0} + \frac{K_a\left(A_{cell} - A_0^{tot}\right)^2}{2A_0^{tot}}, \quad (7)$$

$$V_v = \frac{K_v\left(V_{cell} - V_0^{tot}\right)^2}{2V_0^{tot}}, \quad (8)$$

where K_a, K_d, and K_v are the global area, local area, and volume constraint, respectively. N_t is the number of triangles on the cell membrane. The terms A_{cell} and V_{cell} are the total instant area and volume of the cell, respectively,

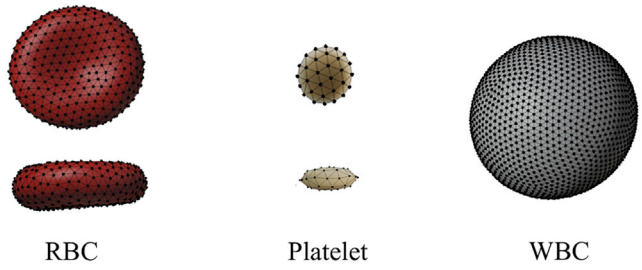

FIGURE 2 Schematics of the RBC, platelet, and WBC models employed in the simulations, which are constructed using 500, 20, and 2000 DPD particles, respectively. To see this figure in color, go online.

while A_0^{tot} and V_0^{tot} are the desired total area and volume, respectively. All constants introduced here are parameterized based on a series of previous studies (79,80) and are summarized in Table S2.

Adhesion model

Inspired by the flow cytometry imaging of blood samples of patients with COVID-19 (33), two different types of CCC models are devised, including WBC and platelet clusters. WBC clusters containing two, three, and four WBCs are examined. Platelet clusters containing four, five, and six platelets are simulated. Dynamical behavior and structural evolution of different blood cells are controlled by various biological and physiological factors such as presence of different proteins in the plasma. Nonetheless, since the lengthscale of these solutes is commonly much smaller compared with those of the cells, it is conventional to coarse grain their effects into an estimated effective interaction rather than explicit modeling of all constituents at all scales, which could be computationally prohibitive. Different surface interactions and effects can be summed into a singular interaction potential that closely mimics the microscopic forces and yields realistic dynamical behavior (81). To consider the adhesion between the cells inside clusters, we apply Morse potential between DPD particles on the blood cells, and it is expressed as

$$U_M(r) = D_e\left[e^{2\beta(r_0-r)} - 2e^{\beta(r_0-r)}\right], \tag{9}$$

where r denotes the distance between two particles, D_e is the depth of the potential well, β denotes the interaction range, and r_0 represents the zero force distance. The Morse potential parameters used for cell-cell interactions are listed in Table S3. Following our previous study (82), when modeling the adhesion between RBCs, the adhesive force is applied to 10%, 50%, and 90% of the particles ("interactive vertices") on each RBC to characterize the impact of the fibrinogen concentration of 4, 6, and 8 mg/mL, respectively, in the whole blood. In the case of WBCs and platelets, the adhesive force is applied to all particles on the cells.

Computational rheometry

Given individual particle velocities and each of the pairwise interactions between particles, the stress tensor, S, can be calculated through the Irving-Kirkwood formalism (83–85).

$$\mathrm{S} = -\frac{1}{V}\left\{\sum_{i=1}^{N} m_i(v_i - u(r_i)) \otimes (v_i - u(r_i)) + \sum_{j>i}^{N}\sum_{i=1}^{N-1} r_{ij} \otimes F_{ij}\right\}, \tag{10}$$

where V is the volume of the entire fluid, N is the total number of atoms in the system, v_i is the velocity of the i-th atom, $u(r_i)$ is the streaming velocity of the i-th atom imposed by the shear flow, m_i represents for mass of the i-th atom, $\otimes$ is the dyadic product of the two vectors, and F_{ij} is the force between the i-th atom and the j-th atom.

Simulation setup

As shown in Fig. 3, all simulations are performed in a rectangular box with a size of 50 μm in each x, y, and z direction. Two flat planes with a thickness of 2 μm are placed in the y direction, and they apply shear to the blood suspension by moving in opposite directions at a constant velocity, which can be tuned to achieve different shear rates. A no-slip boundary condition is implemented on the wall, while periodic boundary conditions are used in the x and z directions. Clusters of WBCs and platelets with three different sizes are randomly placed in the system. RBCs are also filled into the system, and the number of RBCs depends on the selected hematocrit (Ht). Plasma particles are not visualized in the figure for clarity.

Data availability

All simulation data reported in the paper are generated through LAMMPS code https://github.com/AnselGitAccount/USERMESO-2.0-mdpd, and the studied cases can be accessed through https://github.com/procf/Covid-paper_input-files.

RESULTS

In this section, we investigate the impact of different types of CCCs, namely RBC, WBC, and platelet clusters, on the rheology of the blood. First, we simulate the dynamics of CCCs under a range of shear rates that correspond to the physiological values in the microvasculature and veins and measure the viscosity. Then, we identify the critical shear rates that cause the breakup of different types of CCCs. Furthermore, we examine the effects of strength of cell adhesion inside CCCs and the decreased deformability of RBCs on blood viscosity and CCCs splitting.

Dynamics of RBC clusters under shear flow

Blood is a non-Newtonian fluid with shear-thinning properties, which is mainly attributed to rheological properties of RBCs: their deformation under large shear rates and aggregation at low shear rates. In particular, the adhesion between RBCs contributes to the formation of rouleaux, a stack of RBCs clustering into a chain-like structure, at low shear rates. Fibrinogen, a key protein in plasma for blood clotting, plays a vital role in the aggregation of blood cells and the ensuing rouleaux formation (86). A recent microfluidic study (82) has demonstrated that an increased level of fibrinogen in the blood samples of patients with diabetes leads to increased size of the RBC rouleaux. Recent clinical studies have reported that patients with COVID-19 experience a drastic elevation in the level of fibrinogen in their blood

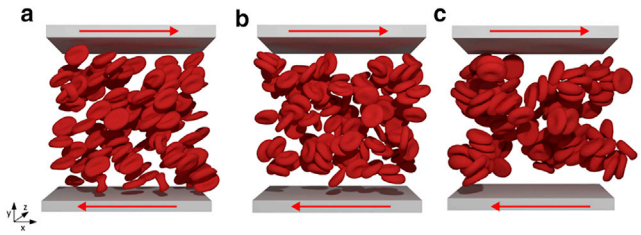

FIGURE 3 Computational modeling of RBC adhesion and aggregation. (*a–c*) Computational simulations modeling RBC adhesion and aggregation with Ht = 10% under shear rates of (*a*) 100 (no cluster), (*b*) 10, and (*c*) 1 s^{-1}. The simulation box is cubic with a size of 50 μm and bounded by two walls of width 2 μm in the pressure gradient direction (*y*). The shear flow is imposed by the bounding walls moving in opposite directions at a constant velocity. The boundary conditions are periodic in the velocity (*x*) and the vorticity (*z*) directions, and a no-slip boundary condition is applied on the walls. To see this figure in color, go online.

(87–90), which likely leads to excessive rouleaux formation under low shear flow in circulation. Furthermore, a new experimental study showed that RBCs from patients with COVID-19 are featured with increased cell stiffness that is 20% higher than the normal subjects (31).

Motivated by these clinical findings, we perform computational simulations to study how the enhanced RBC aggregation and increased RBC stiffness affect blood viscosity. We will test their impact at Ht = 10%, 35%, and 45%, respectively. The steady shear relative viscosity (divided by the plasma viscosity) of cell suspension over a range of shear rates 0.1–1000 s^{-1} is computed. As shown in Fig. 4 *a*, the viscosities at different shear rates computed from our computational model for normal blood at $Ht = 45\%$ is consistent with experimental measurements by Chien et al.(91). The blood viscosity decreases as the Ht is reduced. These results are consistent with our previous work in (45). Additionally, for the case of Ht = 10%, we compute the viscosity in a simulation domain with a size of $100 \times 100 \times 100\ \mu m^3$, eight times larger than the control one ($50 \times 50 \times 50\ \mu m^3$). As shown in Fig. 4 *a*, the computed viscosities from the larger domain are consistent with those calculated from a smaller system, demonstrating the size-independence of our simulation results. See Fig. S1 for the simulation setup of the larger system.

Next, we investigate how the increased fibrinogen contributes to the abnormal hemorheology in COVID-19. Guided by the laboratory studies in (87–90), we compute the blood viscosity with three different fibrinogen concentrations of $c_f = 4$, 6, and 8 mg/mL under the shear rates of 0.1–1000 s^{-1}. To exclude the impact of Ht on elevating the viscosity, the simulation results are normalized by the viscosity of RBC suspension with the same Ht. As shown in Fig. 4 *b*, the increased fibrinogen concentrations could result in up to ~fivefold elevation of the blood viscosity at relative low shear rates due to the RBC agglutination. Particularly, Fig. 3 *b* and *c* illustrate that the size of the RBC cluster increases at a lower shear rate, consistent with findings from prior studies (44,82). Furthermore, we find that the extent of the increase in the viscosity is more pronounced at a higher Ht. On the other hand, when the shear rate is relatively high (>10 s^{-1}), the aggregations break down, and RBCs are dispersed in the system (see Fig. 3 *a*). As a result, RBC adhesion induced by increased fibrinogen concentrations shows no impact on the viscosity of the blood.

Guided by the experimental findings of the RBC biomechanics in COVID-19 in (31), we then increase the rigidity of the RBC model by 20% to examine its effects on blood rheology. Again, the results are normalized by viscosity with the same Ht for normal blood to exclude the impact of Ht. Our results in Fig. 4 *c* show that RBCs with increased rigidity cause an overall increase in blood viscosity, particularly at higher shear rates and larger Ht, but the increases (maximum ~30%) are much smaller than those resulting from the RBC adhesion. Then, we further increase the rigidity of the RBCs by 10-fold, which is comparable to the stiffness of some deoxygenated sickle RBCs in sickle cell disease. Fig. 4 *c* shows that the increased stiffness of RBCs could lead to an elevation of blood viscosity by as much as 80%, in agreement with prior experimental and computational studies (40,92). We note that an increase in RBC rigidity has stronger impact on boosting blood viscosity at higher shear rates where the RBC deformation plays a more dominant role, while at very low shear rates, the

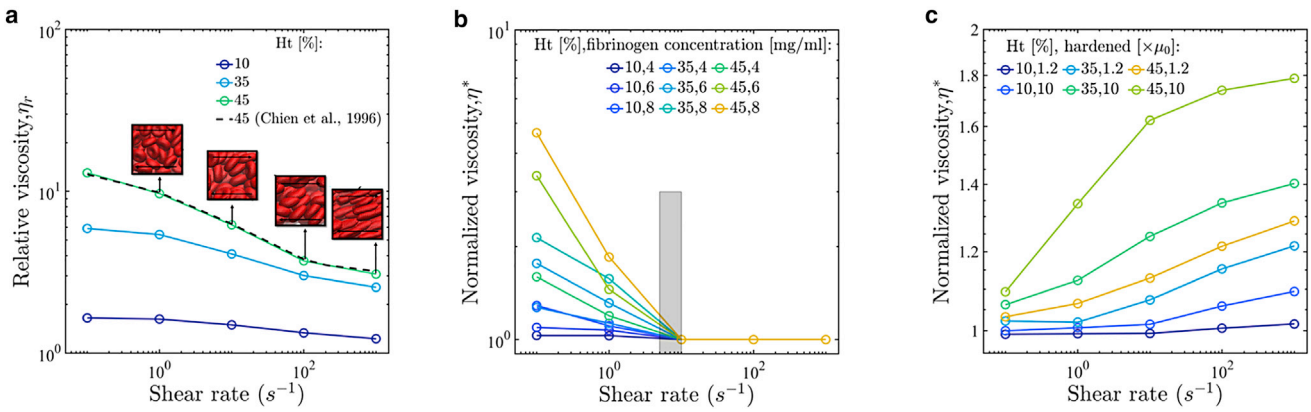

FIGURE 4 Impact of Ht, fibrinogen concentrations, and RBC rigidity on the viscosity of RBC suspension. (*a–c*) Impact of (*a*) Ht, (*b*) fibrinogen concentrations, and (*c*) RBC rigidity on the viscosity of the RBC suspension. Three different Ht, namely Ht = 10%, 35%, and 45%, are examined in (*a*)–(*c*). In (*a*), the relative viscosity is obtained by scaling the computed viscosity with the viscosity of the plasma. The computed relative viscosity for Ht = 45% is compared with experimentally measured viscosity in (91). Simulations of RBC suspension in a simulation box with a size of $100 \times 100 \times 100\ \mu m^3$ are also performed for Ht = 10%. The simulation results (*magenta curve*) are consistent with those calculated from the smaller system ($50 \times 50 \times 50\ \mu m^3$), demonstrating the size independence of our simulation results. In (*b*), three different values of fibrinogen concentrations of $c_f = 4$, 6, and 8 mg/mL are examined. The normalized viscosity is obtained by scaling the computed viscosity with the measurements of the normal RBC suspension at the same Ht without considering the RBC adhesion. The bar signifies the range of the shear rates where the RBC clusters start to break up. In (*c*), the rigidity of RBCs in suspension is increased to 1.2 and 10 times larger than normal RBCs. The normalized viscosity is obtained by scaling the computed viscosity with the measurements of the normal RBC suspension at the same Ht. To see this figure in color, go online.

dynamics of blood flow and the blood rheology are dictated by the interaction between RBCs.

Dynamics of WBC and platelet clusters under shear

Inspired by the flow cytometry images illustrated in Fig. 1, in this section, we simulate the dynamics of WBC clusters containing two, three, and four WBCs under shear flows with shear rates ranging from 0.1 to 1000 s^{-1} as shown in Fig. 5. The computed viscosities for blood containing different sizes of WBC clusters are summarized in Fig. 6, and they are normalized by viscosity with the same Ht for normal blood without WBCs to exclude the impact of Ht. Fig. 6 *a* shows that formation of a WBC cluster could boost the local viscosity of the blood, and the impact of WBCs becomes more pronounced as the number of WBCs inside the clusters and Ht are increased. Next, we examine the impact of increasing the adhesion force between WBCs in CCCs on the blood viscosity. Our results in Fig. 6 *b* show that when the adhesive forces between WBCs are increased to five times larger than the control case, the maximum increase of the viscosity is less than 5%, a much lesser extent than the impact of employing adhesion between RBCs.

Next, we focus on identifying the critical shear rates that can lead to breakup of different WBC clusters. As shown in Fig. 7, the critical shear rate that leads to the splitting of a cluster containing two WBCs is found to be 20 s^{-1}, whereas for clusters consisting of three and four WBCs, a range of shear rates is detected. For instance, one of the three WBCs in the cluster first detaches from the whole cluster at shear rate of 16 s^{-1}, and then the remaining two WBCs break down into single cells at shear rate of 20 s^{-1} (see Fig. 7 *b*). The same range of critical shear rates is also discovered in the case of a cluster containing four WBCs, where the four WBCs first break into two clusters containing two WBCs for each, and then at a critical shear rate of 20 s^{-1}, all four cells are dispersed in the simulation (see Fig. 7 *c*). We further examine these critical shear rates at different levels of Ht and extents of RBC adhesion. Our simulation results show that the critical shear rates causing the breakup of WBC clusters do not change with either the increase in Ht or the enhanced adhesion between RBCs. Next, we compute the critical shear rates when the adhesive force between CCCs is increased due to an elevated fibrinogen concentration in the system. Our results in Fig. 6 *b* show that when the adhesive force between CCCs is increased to two and five times larger than the control case, the critical shear rate is increased to 30–35 and 85–90 s^{-1}, respectively.

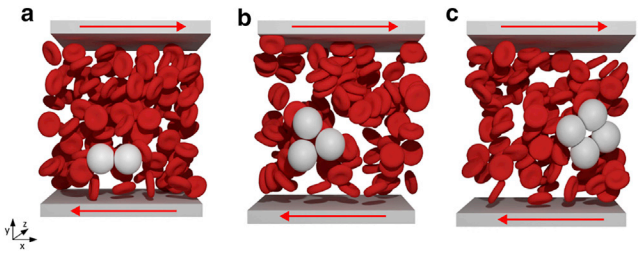

FIGURE 5 Computational modeling of WBC clusters in RBC suspension. (*a–c*) Computational modeling of three different WBC clusters that are composed of (*a*) two, (*b*) three, and (*c*) four WBCs in RBC suspension with Ht = 10% to investigate the impact of WBC clusters on the blood viscosity. To see this figure in color, go online.

Next, we investigate the dynamics of platelet clusters under shear flow with shear rates ranging from 0.1 to 1000 s^{-1}. As illustrated in Fig. 8, platelet clusters that are composed of four, five, and six platelets are examined, respectively. Our simulation results in Fig. 6 *a* show that the impact of these platelet clusters on the viscosity of the blood is negligible with a maximum increase of 1% obtained in the case of a six platelet aggregates inside blood suspension with Ht = 45%, which is likely due to the smaller size of the platelets. Fig. 6 *b* further shows that an increase in the adhesive force between the platelets does not elevate the viscosity. On the other hand, the critical shear rate that causes the breakup of these platelet clusters ranges from 10 to 15 s^{-1}. Fig. 9 *a–c* illustrate that as the shear rate increases, these platelet clusters first are split into smaller clusters and then further separate into individual cells that are dispersed in the system. Similar to the cases of RBC and WBC clusters, an increase in the adhesion force between platelets by two and five times raises the ranges of critical shear rates to 20–25 and 40–45 s^{-1}, respectively (Fig. 6 *b*). We also note that critical shear rates are largely dependent on the adhesion between platelets, and they do not vary with the increasing Ht or the rigidity of RBCs.

DISCUSSION AND SUMMARY

Prominent clinical evidence has demonstrated that COVID-19 could result in a prothrombotic state, which is manifested as venous thrombosis and arterial thrombosis as well as microvascular thrombosis, all of which lead to a negative prognosis. However, the underlying mechanism causing this multiscale thrombus formation is still elusive. Clinical studies have shown that COVID-19-associated hyperviscosity, induced by increased levels of plasma viscosity, could be linked to frequent occurrence of thrombophilia on patients with COVID-19 (32,93). Recent clinical data reported by Choi et al. (94) further demonstrated a significant association between the increased whole-blood viscosity of patients with COVID-19 and higher mortality. This finding implies that in addition to the increased plasma viscosity, the aberrant interaction between blood cells, e.g., increased aggregation of RBCs due to the elevated concentration of fibrinogen in the plasma, could also contribute to the COVID-19-associated hyperviscosity and lead to negative clinical outcomes. In particular, emerging clinical observations of different phenotypes of CCCs, which may block

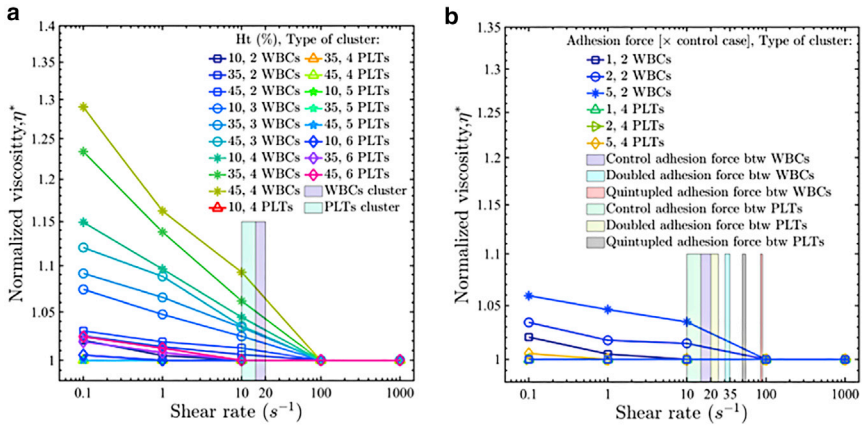

FIGURE 6 Impact of cluster adhesive forces between cells inside CCCs on the viscosity of the blood. Impact of (*a*) WBC and (*b*) platelet cluster adhesive forces between cells inside CCCs on the viscosity of the blood. Three different Ht, namely Ht = 10%, 35%, and 45%, are examined in (*a*) and (*b*). The normalized viscosity is obtained by scaling the computed viscosity with the measurements of the normal RBC suspension at the same Ht. The bars in the figure signify the range of the shear rates where the examined CCCs start to break up. In (*a*), CCC clusters that contain 2, 3, and 4 WBCs and 4, 5, and 6 platelets are examined. In (*b*), the adhesive forces between the cells in CCCs are increased by two- and fivefold, respectively. To see this figure in color, go online.

small blood vessels or act as a nidus for triggering the thrombus formation in circulation (33–36), provided a possible explanation for the ubiquitous prothrombotic state experienced by patients who developed severe COVID-19 symptoms. A recent computational study (95) illustrates that these CCCs could result from an interaction between existing microthrombi and flowing blood cells. For example, a flowing WBC under a strong blood flow could first attach and then detach from a growing platelet aggregate, forming flowing WBC-platelet clusters, while the interaction between a flowing WBC and an adhered WBC leads to formation of a flowing WBC cluster. These observations offer a possible mechanism for the formation of CCCs in the blood of patients with COVID-19 (22,33). However, the adverse effects of these CCCs in the microvasculature have not been systematically investigated.

In the current study, we perform predictive modeling using cellular level blood cell models to explore the impact of different types of CCCs, such as WBC clusters, platelet clusters, and RBC clusters, on the rheology of the blood. First, our simulation results indicate that the increased level of fibrinogen in patients with COVID-19 can promote the formation of RBC clusters at low shear rates, thereby elevating the blood viscosity, a mechanism that also causes the elevation of viscosity in other blood diseases, such as sickle cell disease and type 2 diabetes mellitus. Next, we compute the viscosity of the blood suspension at different Ht in the presence of WBC clusters that are composed of two, three, and four WBCs. We find that the presence of WBC clusters boosts the local viscosity of the blood. In particular, elevation of the viscosity becomes more pronounced when the number of cells inside the clusters is increased. We note that although the increased viscosity in our simulation mainly results from the greater size and larger stiffness of WBCs, making WBCs more resistant to deformation under shear flow, the WBC clusters could also boost the local viscosity by hindering the blood flow through obstructing motion of other cells in microcirculation. Moreover, we introduce platelet clusters, which are also commonly detected in the blood of patients with COVID-19, into the blood suspension and compute the resulting blood viscosity. Our results indicate that the platelet

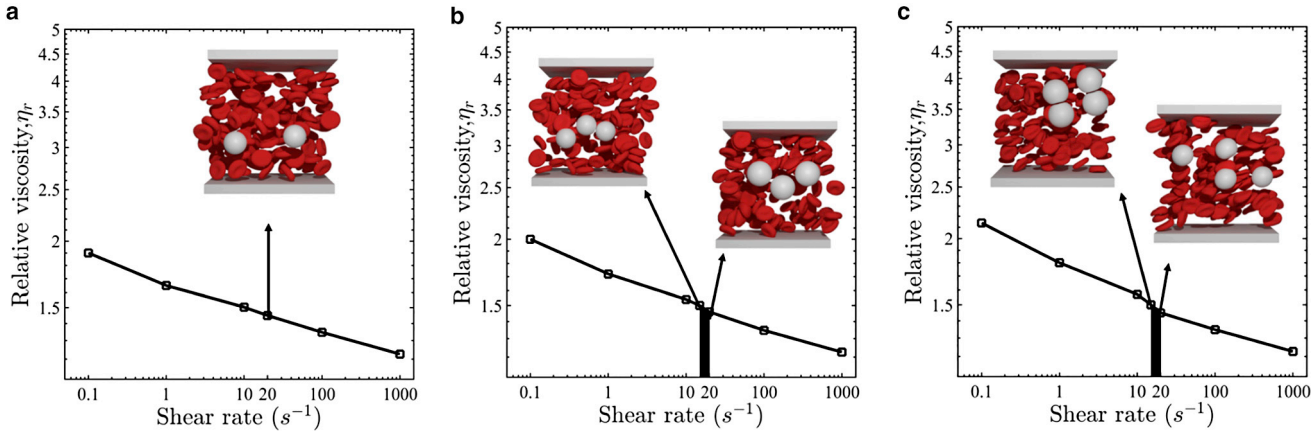

FIGURE 7 Critical shear rates that cause the breakup of the WBC clusters with various sizes. (*a–c*) Critical shear rates causing the breakup of the clusters containing (*a*) two, (*b*) three, and (*c*) four WBCs. The insets in (*b*) and (*c*) show that the WBC clusters first break up into smaller clusters and then are further split into single WBCs. The bars in (*b*) and (*c*) signify the range of the shear rates where the examined CCCs start to break up. To see this figure in color, go online.

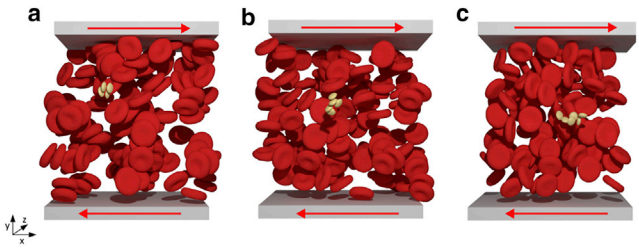

FIGURE 8 Computational modeling of platelet clusters in RBC suspension. (*a–c*) Computational modeling of platelet clusters that are composed of (*a*) four, (*b*) five, and (*c*) six platelets in whole blood with Ht = 10%. To see this figure in color, go online.

clusters do not contribute to the elevated blood viscosity due to the smaller size of the clusters. Furthermore, we assess the critical shear rates that are able to cause the disintegration of these CCCs, and our results show that a larger shear rate is required to break up the WBC cluster than the platelet and RBC clusters. We also find that the critical shear rate could increase from ~20 to ~90 s^{-1} as the adhesion between the cells inside the clusters is enhanced. All these findings imply that while the formation of CCCs has an adverse impact on the microcirculation by altering the blood rheology, WBC clusters are likely to play a more important role in elevating the local blood viscosity. Thus, antiadhesion agents that could prevent the activation and adhesion between WBCs should be considered to improve the microcirculation of patients with COVID-19.

We note that in this study we mainly focus on the biophysical role of WBCs in precipitating the local blood rheology within the microvasculature without considering their biochemical contribution to promoting thrombus formation. Viral invasion could lead to elevated levels of proinflammatory cytokines such as interleukin 6, which can stimulate WBCs (such as monocytes) to synthesize tissue factor (TF) (96), a key mediator for the inflammation-induced coagulation (97), and release TF-positive microparticles that contain adhesion molecule P-selectin glycoprotein ligand-1 (98). These TF-rich microparticles can bind to activated platelets, polymorphonuclear cells (such as neutrophils and eosinophils), and endothelial cells through the counter receptor P-selectin, resulting in activation and expression of TF on these cells (99). Other cytokines, such as tumor necrosis factor-α and interleukin 1, could also induce TF expression on the surfaces of WBCs and endothelial cells (100). The detailed mechanism that causes the formation of CCCs is still elusive. The formation of the RBC clusters could result from the increased level of fibrinogen in patients with COVID-19 as reported in many clinical studies (87–89), a similar mechanism to the formation of rouleaux in the diabetic blood. The adhesion between WBCs and RBCs as well as between platelets could be caused by neutrophil extracellular traps, which are released from the activated neutrophils. As there are no experimental data available for quantifying the adhesive forces between blood cells inside CCCs in COVID-19, we employed the Morse potential between different blood cells, and the parameters of the potential are calibrated based on the dynamics of rouleaux formation and breakup measured in diabetic blood (82). We also vary the magnitude of adhesive forces (two and five times of the benchmark adhesive forces) to quantify the impact of the forces on our simulation results. These model parameters can be further refined upon the availability of experimental data.

In summary, we employ particle-based computational blood cell models to simulate blood suspension over a wide range of physiologically relevant shear rates. The simulation results in the current study improve our understanding of the adverse impact of CCCs in the blood rheology, thereby providing insights into exploring new therapeutic approaches for treating patients with COVID-19. Our study demonstrates that computational modeling can serve as a powerful tool for investigating the pathological alterations of biorheology of blood and their connections to clinical manifestations in infectious diseases, such

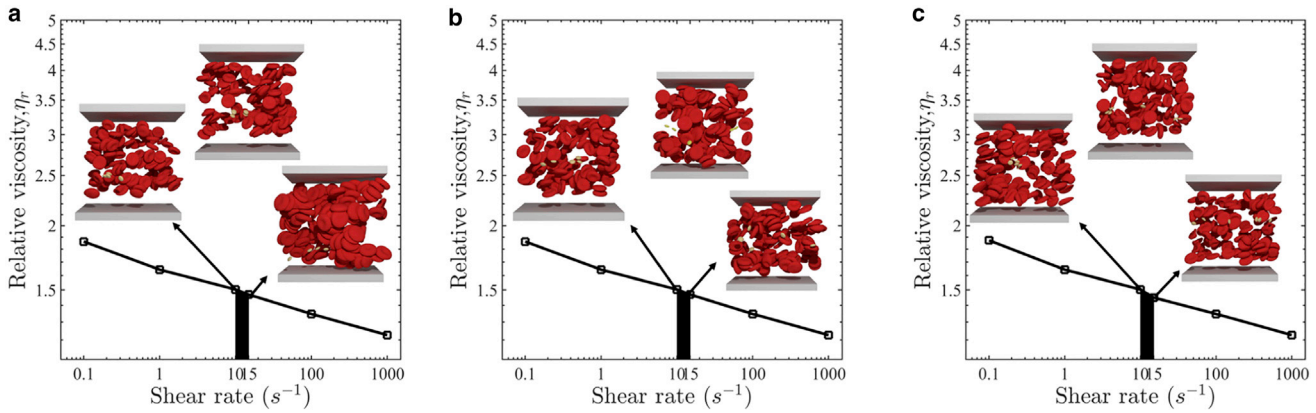

FIGURE 9 Critical shear rates that cause the breakup of the platelet clusters with various sizes. (*a–c*) Critical shear rates causing the breakup of the clusters of (*a*) four, (*b*) five, and (*c*) six platelets. The insets in (*a*)–(*c*) show that the platelet clusters first break up into smaller clusters and then are further split into single platelets. The bars signify the range of the shear rates where the examined CCCs start to break up. To see this figure in color, go online.

as COVID-19, where patients' fresh blood samples are limited for in vitro experimental investigations.

SUPPORTING MATERIAL

Supporting material can be found online at https://doi.org/10.1016/j.bpj.2022.08.031.

AUTHOR CONTRIBUTIONS

E.J., H.L., S.J., and G.E.K. designed the research. E.J. performed the simulations. E.J. and H.L. analyzed the data. E.J., H.L., G.H.F., S.J., and G.E.K. wrote the paper. G.H.F and A.D.G. provided the flow cytometry data.

ACKNOWLEDGMENTS

H.L. and G.E.K. acknowledge the support from National Institutes of Health grant R01HL154150 (https://www.nhlbi.nih.gov/). H.L. acknowledges the support of Richard B. Salomon Award of Brown University (https://www.brown.edu/research/conducting-research-brown/finding-funding/internal-funding-opportunities/ovpr-research-seed-awards). H.L. and G.E.K. acknowledge the support from Extreme Science and Engineering Discovery Environment COVID-19 HPC Consortium, no. TG-BIO200088 (https://www.xsede.org/).

DECLARATION OF INTERESTS

The authors declare no competing interests.

REFERENCES

1. Oxley, T. J., J. Mocco, …, J. T. Fifi. 2020. Large-vessel stroke as a presenting feature of Covid-19 in the young. *N. Engl. J. Med.* 382:e60.
2. Klok, F. A., M. J. H. A. Kruip, …, H. Endeman. 2020. Incidence of thrombotic complications in critically ill ICU patients with COVID-19. *Thromb. Res.* 191:145–147.
3. Akel, T., F. Qaqa, …, F. Shamoon. 2020. Pulmonary embolism: a complication of COVID 19 infection. *Thromb. Res.* 193:79–82.
4. Paterson, R. W., R. L. Brown, …, M. S. Zandi. 2020. The emerging spectrum of COVID-19 neurology: clinical, radiological and laboratory findings. *Brain.* 143:3104–3120.
5. Middeldorp, S., M. Coppens, …, N. van Es. 2020. Incidence of venous thromboembolism in hospitalized patients with COVID-19. *J. Thromb. Haemostasis.* 18:1995–2002.
6. Ali, M. A. M., and S. A. Spinler. 2021. COVID-19 and thrombosis: from bench to bedside. *Trends Cardiovasc. Med.* 31:143–160.
7. Bellosta, R., L. Luzzani, …, G. Piffaretti. 2020. Acute limb ischemia in patients with COVID-19 pneumonia. *J. Vasc. Surg.* 72:1864–1872.
8. Stefanini, G. G., M. Montorfano, …, A. Chieffo. 2020. ST-elevation myocardial infarction in patients with COVID-19: clinical and angiographic outcomes. *Circulation.* 141:2113–2116.
9. Bangalore, S., A. Sharma, …, J. S. Hochman. 2020. ST-segment elevation in patients with Covid-19—a case series. *N. Engl. J. Med.* 382:2478–2480.
10. Mehta, J. L., G. Calcaterra, and P. P. Bassareo. 2020. COVID-19, thromboembolic risk, and Virchow's triad: lesson from the past. *Clin. Cardiol.* 43:1362–1367.
11. Logroscino, G., and E. Beghi. 2021. Stroke epidemiology and COVID-19 pandemic. *Curr. Opin. Neurol.* 34:3–10.
12. Qureshi, A. I., W. I. Baskett, …, C. R. Shyu. 2021. Acute ischemic stroke and covid-19: an analysis of 27 676 patients. *Stroke.* 52:905–912.
13. Virchow, R. 1867. *In* Archiv für pathologische Anatomie und Physiologie und für klinische Medicin, *volume 39*. Reimer.
14. Varga, Z., A. J. Flammer, …, H. Moch. 2020. Endothelial cell infection and endotheliitis in COVID-19. *Lancet.* 395:1417–1418.
15. Singhania, N., S. Bansal, …, G. Singhania. 2020. Current overview on hypercoagulability in COVID-19. *Am. J. Cardiovasc. Drugs.* 20:393–403.
16. Ranucci, M., A. Ballotta, …, L. Menicanti. 2020. The procoagulant pattern of patients with COVID-19 acute respiratory distress syndrome. *J. Thromb. Haemostasis.* 18:1747–1751.
17. Bois, M. C., N. A. Boire, …, J. J. Maleszewski. 2021. COVID-19–associated nonocclusive fibrin microthrombi in the heart. *Circulation.* 143:230–243.
18. Zhao, C. L., A. Rapkiewicz, …, I. Hanna. 2021. Pathological findings in the postmortem liver of patients with coronavirus disease 2019 (COVID-19). *Hum. Pathol.* 109:59–68.
19. Rapkiewicz, A. V., X. Mai, …, H. R. Reynolds. 2020. Megakaryocytes and platelet-fibrin thrombi characterize multi-organ thrombosis at autopsy in COVID-19: a case series. *EClinicalMedicine.* 24:100434.
20. Fox, S. E., A. Akmatbekov, …, R. S. Vander Heide. 2020. Pulmonary and cardiac pathology in African American patients with COVID-19: an autopsy series from New Orleans. *Lancet Respir. Med.* 8:681–686.
21. Diao, B., C. Wang, …, Y. Chen. 2021. Human kidney is a target for novel severe acute respiratory syndrome coronavirus 2 infection. *Nat. Commun.* 12:2506–2509.
22. McFadyen, J. D., H. Stevens, and K. Peter. 2020. The emerging threat of (micro) thrombosis in COVID-19 and its therapeutic implications. *Circ. Res.* 127:571–587.
23. Helms, J., C. Tacquard, …, F. Meziani. 2020. High risk of thrombosis in patients with severe SARS-CoV-2 infection: a multicenter prospective cohort study. *Intensive Care Med.* 46:1089–1098.
24. Lowe, G. D. 1992. Blood viscosity and cardiovascular disease. *Thromb. Haemostasis.* 67:494–498.
25. Litvinov, R. I., and J. W. Weisel. 2017. Role of red blood cells in haemostasis and thrombosis. *ISBT Sci. Ser.* 12:176–183.
26. Byrnes, J. R., and A. S. Wolberg. 2017. Red blood cells in thrombosis. *Blood.* 130:1795–1799.
27. De Franceschi, L., M. D. Cappellini, and O. Olivieri. 2011. Thrombosis and sickle cell disease. *Semin. Thromb. Hemost.* 37:226–236. Thieme Medical Publishers.
28. Musallam, K. M., and A. T. Taher. 2011. Thrombosis in thalassemia: why are we so concerned? *Hemoglobin.* 35:503–510.
29. Vazzana, N., P. Ranalli, …, G. Davì. 2012. Diabetes mellitus and thrombosis. *Thromb. Res.* 129:371–377.
30. Chapin, J., H. S. Terry, …, J. Laurence. 2016. The role of complement activation in thrombosis and hemolytic anemias. *Transfus. Apher. Sci.* 54:191–198.
31. Kubánková, M., B. Hohberger, …, M. Kräter. 2021. Physical phenotype of blood cells is altered in COVID-19. *Biophys. J.* 120:2838–2847.
32. Nader, E., C. Nougier, …, P. Connes. 2022. Increased blood viscosity and red blood cell aggregation in patients with COVID-19. *Am. J. Hematol.* 97:283–292.
33. Dorken Gallastegi, A., L. Naar, …, R. Tompkins. 2021. Circulating cellular clusters are correlated with thrombotic complications and clinical outcomes in COVID-19. *In* Research and Practice in Thrombosis and Haemostasis.
34. Le Joncour, A., L. Biard, …, D. Saadoun. 2020. Neutrophil–platelet and monocyte–platelet aggregates in COVID-19 patients. *Thromb. Haemostasis.* 120:1733–1735.

35. do Espírito Santo, D. A., A. C. B. Lemos, and C. H. Miranda. 2020. In vivo demonstration of microvascular thrombosis in severe COVID-19. *J. Thromb. Thrombolysis.* 50:790–794.

36. Nicolai, L., A. Leunig, …, K. Stark. 2020. Immunothrombotic dysregulation in COVID-19 pneumonia is associated with respiratory failure and coagulopathy. *Circulation.* 142:1176–1189.

37. Rosencranz, R., and S. A. Bogen. 2006. Clinical laboratory measurement of serum, plasma, and blood viscosity. *Am. J. Clin. Pathol.* 125:S78–S86.

38. Beris, A. N., J. S. Horner, …, N. J. Wagner. 2021. Recent advances in blood rheology: a review. *Soft Matter.* 17:10591–10613.

39. Ye, T., N. Phan-Thien, and C. T. Lim. 2016. Particle-based simulations of red blood cells—a review. *J. Biomech.* 49:2255–2266.

40. Li, X., H. Li, …, G. Em Karniadakis. 2017. Computational biomechanics of human red blood cells in hematological disorders. *J. Biomech. Eng.* 139:0210081.

41. Li, H., D. P. Papageorgiou, …, Y. Deng. 2018. Synergistic integration of laboratory and numerical approaches in studies of the biomechanics of diseased red blood cells. *Biosensors.* 8:76.

42. Li, H., H. Y. Chang, …, G. Lykotrafitis. 2018. Modeling biomembranes and red blood cells by coarse-grained particle methods. *Appl. Math. Mech.* 39:3–20.

43. Deng, Y. X., H.-y. Chang, and H. Li. 2022. Recent advances in computational modeling of biomechanics and biorheology of red blood cells in diabetes. *Biomimetics.* 7:15.

44. Fedosov, D. A., W. Pan, …, G. E. Karniadakis. 2011. Predicting human blood viscosity in silico. *Proc. Natl. Acad. Sci. USA.* 108:11772–11777.

45. Javadi, E., Y. Deng, …, S. Jamali. 2021. In silico biophysics and hemorheology of blood hyperviscosity syndrome. *Biophys. J.* 120:2723–2733.

46. Javadi, E., and S. Jamali. 2021. Hemorheology: the critical role of flow type in blood viscosity measurements. *Soft Matter.* 17:8446–8458.

47. Liu, Z. L., H. Li, …, G. E. Karniadakis. 2021. Computational modeling of biomechanics and biorheology of heated red blood cells. *Biophys. J.* 120:4663–4671.

48. Lei, H., and G. E. Karniadakis. 2012. Quantifying the rheological and hemodynamic characteristics of sickle cell anemia. *Biophys. J.* 102:185–194.

49. Li, H., and G. Lykotrafitis. 2011. A coarse-grain molecular dynamics model for sickle hemoglobin fibers. *J. Mech. Behav. Biomed. Mater.* 4:162–173.

50. Li, H., V. Ha, and G. Lykotrafitis. 2012. Modeling sickle hemoglobin fibers as one chain of coarse-grained particles. *J. Biomech.* 45:1947–1951.

51. Lu, L., H. Li, …, G. E. Karniadakis. 2017. Mesoscopic adaptive resolution scheme toward understanding of interactions between sickle cell fibers. *Biophys. J.* 113:48–59.

52. Perazzo, A., Z. Peng, …, H. A. Stone. 2022. The effect of rigid cells on blood viscosity: linking rheology and sickle cell anemia. *Soft Matter.* 18:554–565.

53. Chang, H.-Y., X. Li, and G. E. Karniadakis. 2017. Modeling of biomechanics and biorheology of red blood cells in type 2 diabetes mellitus. *Biophys. J.* 113:481–490.

54. Javadi, E., and S. Jamali. 2022. Thixotropy and rheological hysteresis in blood flow. *J. Chem. Phys.* 156:084901.

55. Li, H., and G. Lykotrafitis. 2012. Two-component coarse-grained molecular-dynamics model for the human erythrocyte membrane. *Biophys. J.* 102:75–84.

56. Li, H., and G. Lykotrafitis. 2014. Erythrocyte membrane model with explicit description of the lipid bilayer and the spectrin network. *Biophys. J.* 107:642–653.

57. Tang, Y. H., L. Lu, …, G. E. Karniadakis. 2017. OpenRBC: a fast simulator of red blood cells at protein resolution. *Biophys. J.* 112:2030–2037.

58. Zhang, P., L. Zhang, …, D. Bluestein. 2017. A multiscale biomechanical model of platelets: correlating with in-vitro results. *J. Biomech.* 50:26–33.

59. Li, H., J. Yang, …, G. E. Karniadakis. 2018. Cytoskeleton remodeling induces membrane stiffness and stability changes of maturing reticulocytes. *Biophys. J.* 114:2014–2023.

60. Li, H., L. Lu, …, S. Suresh. 2018. Mechanics of diseased red blood cells in human spleen and consequences for hereditary blood disorders. *Proc. Natl. Acad. Sci. USA.* 115:9574–9579.

61. Chang, H. Y., X. Li, …, G. E. Karniadakis. 2016. MD/DPD multiscale framework for predicting morphology and stresses of red blood cells in health and disease. *PLoS Comput. Biol.* 12:e1005173.

62. Dearnley, M., T. Chu, …, L. Tilley. 2016. Reversible host cell remodeling underpins deformability changes in malaria parasite sexual blood stages. *Proc. Natl. Acad. Sci. USA.* 113:4800–4805.

63. Li, H., and G. Lykotrafitis. 2015. Vesiculation of healthy and defective red blood cells. *Phys. Rev. E Stat. Nonlin. Soft Matter Phys.* 92:012715.

64. Li, H., Z. L. Liu, …, G. E. Karniadakis. 2021. How the spleen reshapes and retains young and old red blood cells: a computational investigation. *PLoS Comput. Biol.* 17:e1009516.

65. Pivkin, I. V., and G. E. Karniadakis. 2008. Accurate coarse-grained modeling of red blood cells. *Phys. Rev. Lett.* 101:118105.

66. Geekiyanage, N. M., M. A. Balanant, …, Y. Gu. 2019. A coarse-grained red blood cell membrane model to study stomatocyte-discocyte-echinocyte morphologies. *PLoS One.* 14:e0215447.

67. Geekiyanage, N., E. Sauret, …, Y. Gu. 2020. Modelling of red blood cell morphological and deformability changes during in-vitro storage. *Appl. Sci.* 10:3209.

68. Li, H., Y. Deng, …, G. E. Karniadakis. 2022. Computational investigation of blood cell transport in retinal microaneurysms. *PLoS Comput. Biol.* 18:e1009728.

69. Yazdani, A., Y. Deng, …, G. Em Karniadakis. 2021. Integrating blood cell mechanics, platelet adhesive dynamics and coagulation cascade for modelling thrombus formation in normal and diabetic blood. *J. R. Soc. Interface.* 18:20200834.

70. Czaja, B., J. de Bouter, A. Hoekstra…, 2022. The effect of stiffened diabetic red blood cells on wall shear stress in a reconstructed 3D microaneurysm. *Comput. Methods Biomech. Biomed. Eng.* 25:1–19. https://doi.org/10.1080/10255842.2022.2034794.

71. Závodszky, G., B. Van Rooij, …, A. Hoekstra. 2017. Cellular level in-silico modeling of blood rheology with an improved material model for red blood cells. *Front. Physiol.* 8:563.

72. Fedosov, D. A., B. Caswell, and G. E. Karniadakis. 2010. A multiscale red blood cell model with accurate mechanics, rheology, and dynamics. *Biophys. J.* 98:2215–2225.

73. Español, P. 1997. Dissipative particle dynamics with energy conservation. *Europhys. Lett.* 40:631–636.

74. Boey, S. K., D. H. Boal, and D. E. Discher. 1998. Simulations of the erythrocyte cytoskeleton at large deformation. I. Microscopic models. *Biophys. J.* 75:1573–1583.

75. Fedosov, D. A., M. Peltomäki, and G. Gompper. 2014. Deformation and dynamics of red blood cells in flow through cylindrical microchannels. *Soft Matter.* 10:4258–4267.

76. Noguchi, H., and G. Gompper. 2004. Fluid vesicles with viscous membranes in shear flow. *Phys. Rev. Lett.* 93:258102.

77. Noguchi, H., and G. Gompper. 2005. Shape transitions of fluid vesicles and red blood cells in capillary flows. *Proc. Natl. Acad. Sci. USA.* 102:14159–14164.

78. Ebrahimi, S., and P. Bagchi. 2022. A computational study of red blood cell deformability effect on hemodynamic alteration in capillary vessel networks. *Sci. Rep.* 12:4304–4319.

79. Chang, H. Y., A. Yazdani, …, G. E. Karniadakis. 2018. Quantifying platelet margination in diabetic blood flow. *Biophys. J.* 115:1371–1382.

80. Lei, H., and G. E. Karniadakis. 2013. Probing vasoocclusion phenomena in sickle cell anemia via mesoscopic simulations. *Proc. Natl. Acad. Sci. USA.* 110:11326–11330.

81. Israelachvili, J. N. 2011. Intermolecular and Surface Forces. Academic press.

82. Deng, Y., D. P. Papageorgiou, …, G. E. Karniadakis. 2020. Quantifying fibrinogen-dependent aggregation of red blood cells in type 2 diabetes mellitus. *Biophys. J.* 119:900–912.

83. Irving, J. H., and J. G. Kirkwood. 1950. The statistical mechanical theory of transport processes. IV. The equations of hydrodynamics. *J. Chem. Phys.* 18:817–829.

84. Jamali, S., A. Boromand, …, J. Maia. 2015. Microstructure and rheology of soft to rigid shear-thickening colloidal suspensions. *J. Rheol.* 59:1377–1395.

85. Boromand, A., S. Jamali, and J. M. Maia. 2015. Viscosity measurement techniques in dissipative particle dynamics. *Comput. Phys. Commun.* 196:149–160.

86. Krüger-Genge, A., R. Sternitzky, …, F. Jung. 2019. Erythrocyte aggregation in relation to plasma proteins and lipids. *J. Cell. Biotechnol.* 5:65–70.

87. Masi, P., G. Hékimian, …, C. Frere. 2020. Systemic inflammatory response syndrome is a major contributor to COVID-19–associated coagulopathy: insights from a prospective, single-center cohort study. *Circulation.* 142:611–614.

88. Patel, B. V., D. J. Arachchillage, …, S. R. Desai. 2020. Pulmonary angiopathy in severe COVID-19: physiologic, imaging, and hematologic observations. *Am. J. Respir. Crit. Care Med.* 202:690–699.

89. Panigada, M., N. Bottino, …, A. Tripodi. 2020. Hypercoagulability of COVID-19 patients in intensive care unit: a report of thromboelastography findings and other parameters of hemostasis. *J. Thromb. Haemostasis.* 18:1738–1742.

90. Spiezia, L., A. Boscolo, …, P. Simioni. 2020. COVID-19-related severe hypercoagulability in patients admitted to intensive care unit for acute respiratory failure. *Thromb. Haemostasis.* 120:998–1000.

91. Chien, S., S. Usami, …, M. I. Gregersen. 1966. Effects of hematocrit and plasma proteins on human blood rheology at low shear rates. *J. Appl. Physiol.* 21:81–87.

92. Kaul, D. K., M. E. Fabry, …, R. L. Nagel. 1983. Erythrocytes in sickle cell anemia are heterogeneous in their rheological and hemodynamic characteristics. *J. Clin. Invest.* 72:22–31.

93. Maier, C. L., A. D. Truong, …, A. Duncan. 2020. COVID-19-associated hyperviscosity: a link between inflammation and thrombophilia? *Lancet.* 395:1758–1759.

94. Choi, D., O. Waksman, …, R. S. Rosenson. 2022. Association of blood viscosity with mortality among patients hospitalized with COVID-19. *J. Am. Coll. Cardiol.* 80:316–328.

95. Li, H., Y. Deng, Z. Li, …, G. E. Karniadakis. 2022. Multiphysics and multiscale modeling of microthrombosis in COVID-19. *PLoS Comput. Biol.* 18:e1009892.

96. Neumann, F.-J., I. Ott, …, A. Schömig. 1997. Effect of human recombinant interleukin-6 and interleukin-8 on monocyte procoagulant activity. *Arterioscler. Thromb. Vasc. Biol.* 17:3399–3405.

97. Levi, M., T. van der Poll, and H. R. Büller. 2004. Bidirectional relation between inflammation and coagulation. *Circulation.* 109:2698–2704.

98. Rauch, U., D. Bonderman, …, Y. Nemerson. 2000. Transfer of tissue factor from leukocytes to platelets is mediated by CD15 and tissue factor. *Blood.* 96:170–175.

99. Derhaschnig, U., D. Bergmair, …, B. Jilma. 2004. Effect of interleukin-6 blockade on tissue factor-induced coagulation in human endotoxemia. *Crit. Care Med.* 32:1136–1140.

100. Kirchhofer, D., T. B. Tschopp, …, H. R. Baumgartner. 1994. Endothelial cells stimulated with tumor necrosis factor-alpha express varying amounts of tissue factor resulting in inhomogenous fibrin deposition in a native blood flow system. Effects of thrombin inhibitors. *J. Clin. Invest.* 93:2073–2083.